Numerical and Laboratory Study of Horizontally Evolving Convective Boundary Layer. Part II: Effects of Elevated Wind Shear and Surface Roughness

E. FEDOROVICH

Institute for Hydromechanics, University of Karlsruhe, Karlsruhe, Germany

F. T. M. NIEUWSTADT

J. M. Burgers Centre for Fluid Mechanics, Delft University of Technology, Delft, Netherlands

R. KAISER

Zeuna Stärker GmbH & Co. KG, Augsburg, Germany

(Manuscript received 15 November 1999, in final form 26 April 2000)

ABSTRACT

Modifications of turbulence regime in the sheared convective boundary layer (CBL) by a number of external nonbuoyant forcings are studied experimentally in a thermally stratified wind tunnel and numerically by means of large eddy simulation. This type of CBL is observed in the atmosphere when an originally neutral or stable air mass is advected over a heated underlying surface. Emphasis in the present study is laid on the effects of elevated wind shear and surface roughness on the structure and evolution of the CBL. For the flow cases, for which both numerical and wind tunnel results are available, the numerical predictions of mean flow parameters and turbulence statistics are found to be in good agreement with the experimental results.

In the case of wind shear across the inversion layer, the authors distinguish between positive shear, when the flow above the inversion possesses a higher momentum than mean motion in the mixed layer, and the opposite case of negative shear. For the case of positive shear the growth of the CBL is found to be impeded compared to the shear-free case. Negative shear has an opposite effect on the CBL evolution. In this case, the damping of thermals by stable stratification in the inversion layer is weakened compared to the shear-free case and consequently entrainment is activated. A physical explanation for such a directional effect of elevated shear is suggested. In the case of enhanced bottom roughness, both experiments and numerical simulations provide the evidence of slightly larger CBL growth rate compared to the CBL over a relatively smooth surface with a 10 times smaller roughness length.

1. Introduction

The dry atmospheric convective boundary layer (CBL) is an example of buoyancy-driven flow with a broad spectrum of interacting mechanisms contributing to the mean flow and turbulence. Investigation of the turbulence structure in the CBL, and its adequate description (parameterization), is of importance for environmental atmospheric research, for weather and climate forecasting, and for understanding of the fundamental properties of turbulence in convective geophysical flows.

Field observations, laboratory modeling, and numerical simulation are established techniques to study turbulence in the atmospheric CBL. Each of these approaches possesses certain advantages and deficiencies. In order to ensure the progress of atmospheric CBL research, the aforementioned tools should be used in combination, as was emphasized by Wyngaard (1998), so that they can mutually complement each other.

In the present study, the laboratory (wind tunnel) modeling and numerical simulation [large eddy simulation (LES)] are employed in combination to study the structure of the horizontally evolving CBL. Data from measurements in the atmospheric CBL have been used in the first part of this study (Fedorovich et al. 2001, hereafter referred to as FNK1) to verify results of the numerical simulations and laboratory experiments. That part of the study has further focused on the transition regimes in the evolving CBL and on features of turbulence structure in the developed convectively mixed layer.

As noted in FNK1, most numerical and laboratory

Corresponding author address: Dr. Evgeni Fedorovich, School of Meteorology, University of Oklahoma, Energy Center, 100 East Boyd, Norman, OK 73019-1013.
E-mail: fedorovich@ou.edu

model studies carried out so far have concentrated on the case of the horizontally homogeneous, nonsteady CBL. In these studies, the main topic of investigation has been the principal CBL forcing, which is the convective heat transfer from the warm underlying surface. Just a few studies have been devoted to the investigation of effects produced by additional nonconvective (or nonbuoyant) forcings that contribute to the CBL turbulence regime in conjunction with the dominant driving mechanism of buoyant convection. Examples of such forcings are wind shears, both at the surface and across the inversion at the top of the boundary layer, and surface roughness.

Let us first consider wind shears. The effect of surface shear on convection was investigated by means of LES in a study of Sykes and Henn (1989). Although the case studied was not exactly relevant to the atmospheric CBL, the results obtained have nevertheless provided a quantitative estimate of the ability of an externally applied shear to organize the convective eddies into two-dimensional rolls. Combined effects of wind shear and buoyancy forces in the atmospheric CBL have been studied numerically by Moeng and Sullivan (1994). They observed a similar reorganization of the turbulence structure when the shear-free convection regime in the boundary layer has been replaced by the sheared convection. As the contribution of wind shear grows, elongated streaks of high and low speed are formed in the near-surface region of the simulated boundary layer flow replacing the irregular polygonal structure characteristic of the shear-free convective flow. Mason (1992) applied LES to study dispersion of a passive scalar in a CBL with wind shear. He found that a relative increase of shear with respect to buoyancy led to an increase of short-time dispersion rates. In contrast, the vertical dispersion at greater time was reduced and took on the character of a simple diffusive process. Mason linked this marked change in vertical dispersion to the effect of a reduced length scale in shear-driven turbulence compared with convective turbulence.

In the studies quoted above, the ratio of the friction velocity u_* to the convective velocity scale w_* was identified as an important parameter that determines the formation of longitudinal rolls and describes the modification of turbulence statistics in the sheared convective flow. For $u_*/w_* < 0.3$, the CBL flow properties were found to be close to the shear-free convection. With $u_*/w_* > 0.35$, rolls start to form in the CBL, and turbulence statistics such as velocity variances deviate noticeably from their values in the free-convection case. In some other atmospheric boundary layer studies (see, for instance Holtslag and Nieuwstadt 1986), another parameter, namely, the ratio between the Monin–Obukhov length scale and the CBL depth, $-L/z_i$, has been selected to characterize the relative contribution of surface shear and buoyancy to the turbulence production in the CBL. It can be shown that $u_*/w_* = -(kL/z_i)^{1/3}$, where $k = 0.4$ is the von Kármán constant. For the value of $-L/z_i$ separating the regimes of shear-free and sheared convection Holtslag and Nieuwstadt (1986) proposed 0.1, which corresponds approximately to $u_*/w_* = 0.34$. This value is well in agreement with the above presented estimates of the critical value for u_*/w_* obtained from LES.

A comprehensive LES study of the three-dimensional structure of buoyancy- and shear-induced turbulence in the atmospheric boundary layer has been conducted by Khanna and Brasseur (1998). Their computations spanned a vast range of stability conditions starting from a nearly shear-free CBL ($-L/z_i = 0.0014$, $u_*/w_* = 0.0047$) to an almost purely shear-driven boundary layer ($-L/z_i = 2.3$, $u_*/w_* = 7.7$). Besides general support of earlier findings by Moeng and Sullivan (1994) concerning the shear-induced alteration of the CBL coherent structure, this study provided insights into the individual properties of convective thermals and rolls.

Based on the comparison of visualizations of structures with turbulence spectra in the buoyancy-driven flow, Khanna and Brasseur (1998) have shown that the disparity in the near-ground horizontal scale between temperature and vertical velocity reflects the structure of more localized thermals within the large-scale cells. Several features of the near-ground shear-induced regions of high- and low-speed flow in the sheared boundary layer have been examined. An interaction between z_i-scale outer eddies and near-ground streaks has been identified, with a tendency toward strengthening at smaller $-L/z_i$. Warm fluid accumulated in low-speed streaks has been found to be accelerated upward by localized buoyancy forces within sheets aligned with the mean wind. These sheetlike updrafts constitute the ascending component of large-scale streamwise roll-like motion that embrace the whole CBL. Based on these observations, Khanna and Brasseur concluded that the shear-dominated near-surface structure of the unstable surface layer influences directly the global structure of the moderately convective boundary layer.

Modification of the CBL turbulence regime by surface shear has been investigated experimentally by Fedorovich et al. (1996) and Kaiser and Fedorovich (1998) in a wind tunnel model of a horizontally evolving CBL. Surface flow shear was found to be an essential part of the turbulence production. Values of the surface shear-to-buoyancy production ratio u_*/w_* of 0.3 and more resulted in a noticeable increase in the variance of velocity fluctuations in the lower portion of the layer compared with their counterparts in the shear-free CBL. Weak roll-like semiorganized motions were identified in the pattern of mean velocity measured in planes perpendicular to the mean flow direction. In the bulk of the CBL, the buoyancy was found to be the dominant factor of turbulence production at smaller wavenumbers, while the shear contribution was apparently increasing with at the large wavenumbers. The combined effect of buoyant and shear forcings in the simulated CBL was suggested to be a reason for the elongation and flatness

of the production ranges in the measured velocity spectra.

Compared to the effect of shear at the surface, the influence of wind shear across the capping inversion (the so-called elevated shear) on turbulence in the CBL is much less studied. Such shear is typically observed in the atmospheric CBL under baroclinic conditions (Stull 1988). The velocity increments across the inversion layer in the baroclinic CBL can be of either sign depending on the geostrophic wind change with height in terms of the so-called thermal wind (Fedorovich 1995).

In bulk models of the CBL, the contribution of elevated shear to the energy balance integrated across the boundary layer is parameterized through an additional term in the entrainment equation that describes boundary layer growth (Fedorovich 1998). If the inversion layer is represented by zero-order discontinuity interface, this contribution is proportional, as shown in Fedorovich (1995), to the product of the velocity increment across this interface to the second power and the rate of the CBL growth (the so-called entrainment rate, dz_i/dt). Thus, according to the zero-order jump approach, the contribution of elevated shear to production of the turbulent kinetic energy in the growing CBL ($dz_i/dt > 0$) is essentially positive.

Wind tunnel measurements of Fedorovich and Kaiser (1998) have provided an indication, however, that turbulence enhancement in the upper portion of CBL with elevated shear may be accompanied by the decrease of the CBL growth rate. To a certain extent, such damping of entrainment by elevated shear can be related to the so-called shear sheltering of turbulence. Analyses of this phenomenon were presented by Jacobs and Durbin (1998), and Hunt and Durbin (1999), and in connection with crosswind effects in the inversion layer by Hunt (1998).

Due to technical restrictions, the experiments of Fedorovich and Kaiser (1998) could be conducted only with positive shear across the inversion layer, when the flow in the outer turbulence-free region has larger mean momentum than the turbulent flow in the bulk of the CBL. As will be shown below, in the case of negative elevated shear (when the fluid below the inversion moves faster than the fluid above the inversion) the effect of elevated shear on the CBL growth is quite different.

Another mechanism of turbulence enhancement in the CBL is associated with roughness elements at the underlying surface. This mechanism is closely related to the production of turbulence by surface shear because they are both of mechanical nature. Surface roughness affects the flow through pressure drag forces produced by individual roughness elements and through viscous forces associated with the no-slip conditions on the surface of these elements.

In numerical studies of atmospheric convection, the effect of surface roughness is often disregarded owing to negligible turbulence generated by it compared with the generation of turbulence by buoyancy forces (see, for instance, Cai 1999). There is nevertheless no experimental evidence available whether it is really the case. Following Khanna and Brasseur (1998) one may assume that the surface roughness (especially, when it is large, e.g., in the case of an urban surface) can considerably change the flow regime in the surface layer and thus may affect the large-scale convective motions. Also, the analysis presented by Zilitinkevich et al. (1998) has shown that properties of momentum and heat exchange in the convective surface layer are essentially dependent on the ratio of the roughness length to the CBL depth.

To further clarify the effects of elevated shear and surface roughness, we investigate in the present study the turbulence regime of the horizontally evolving CBL. It is done experimentally, in the thermally stratified wind tunnel of the University of Karlsruhe (UniKa), and numerically, by means of the LES technique described in FNK1. The objectives of our study are (i) to quantify the effects of elevated shear and surface roughness on the turbulence structure and on the entrainment in the CBL, and (ii) to provide insights in the physical mechanisms of these effects.

The outline of the paper is as follows. In section 2, the investigated flow regimes will be overviewed. In the two subsequent sections, we will focus on the laboratory and numerical results for the cases with elevated shear (section 3) and with enhanced surface roughness (section 4). Section 5 will be devoted to discussion, summarizing remarks, and conclusions.

2. Investigated flow regimes

The flow cases that we have selected for our study are illustrated in Fig. 1. For the details of the experimental and numerical techniques used to obtain the data for these flow cases we refer to FNK1.

The reference case, to which we shall relate our results discussed in the following sections of the paper, is called the basic flow configuration (BFC). It has been comprehensively presented and discussed in FNK1. Some more characteristics of the CBL turbulence regime in this case and description of the flow measurement technique (including accuracy considerations) can be found in Fedorovich et al. 1996, Kaiser and Fedorovich (1998), and Fedorovich and Kaiser (1998).

In the BFC, the two lower layers of the tunnel, with a depth of 0.3 m in total, are operated in the open-circuit regime with the incoming flow possessing the temperature of the ambient air (about 300 K). When the BFC has been reproduced numerically, random temperature fluctuations with prescribed rms value have been added to the inflow mean temperature field in these two layers in order to simulate uncontrolled flow disturbances in the open section of the wind tunnel (see FNK1). Between the second and the third layers in the tunnel a

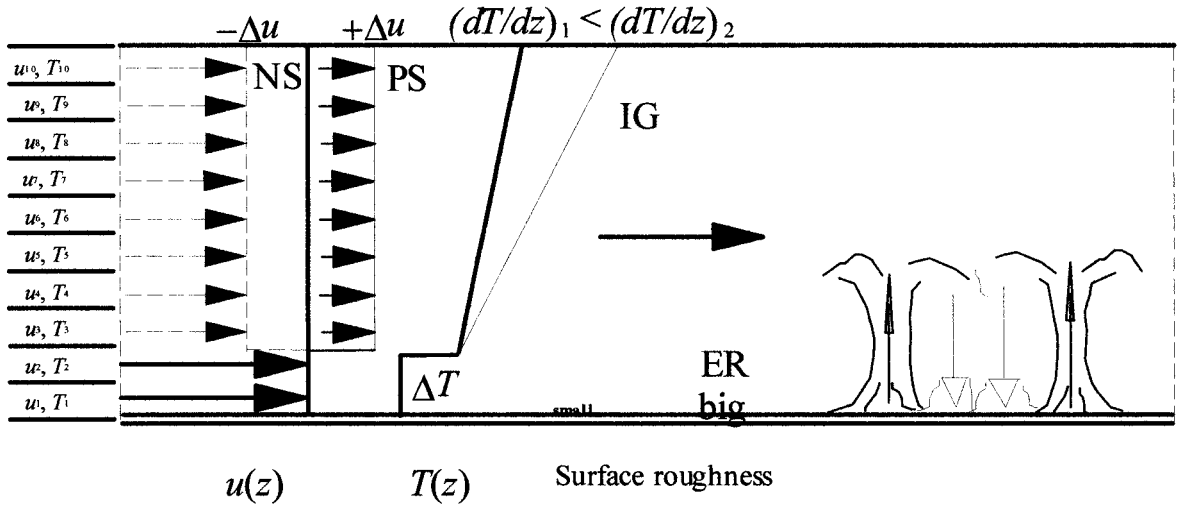

FIG. 1. Sketch of investigated flow regimes with different forcings. The basic flow configuration (BFC) is shown by bold lines and symbols. Case I (positive elevated shear) is indicated as PS. Case II (negative elevated shear) is indicated as NS. Case III (enhanced surface roughness) is denoted as ER. The supplementary case with increased temperature gradient above the inversion is indicated as IG.

temperature jump of 30 K has been imposed. The temperatures of the subsequent layers have been controlled in a way to produce a temperature gradient of 33 K m^{-1} (5 K $layer^{-1}$) in the upper flow region. In this flow portion, a stationary inflow boundary condition for the temperature field has been prescribed in the numerical simulation of BFC (see FNK1). The inlet flow velocity in all layers has been set equal to 1 m s^{-1}. This value has been taken as stationary inflow boundary condition for the velocity field in the numerical simulation of BFC (see FNK1). The kinematic heat flux through the wind tunnel floor has been kept constant, at the level of approximately 1 K m s^{-1}.

Let us now consider in more detail the different flow regimes that we aim to study.

Case I is a flow configuration with positive elevated shear (PS). In this case, the velocity across the CBL top increases from 1.0 m s^{-1} in the boundary layer to a value of 1.5 m s^{-1} in the outer layer. The remaining parameters are kept equal to those of the BFC. In other words, an elevated shear of 0.5 m s^{-1} is imposed in the incoming flow at the capping inversion level $z = 0.3$ m.

Case II is a flow configuration with negative elevated shear (NS). In the incoming flow below the inversion the mean velocity u is kept equal to 1.0 m s^{-1}. Above the inversion, it is set equal to 0.5 m s^{-1}. Thus, a negative elevated shear of -0.5 m s^{-1} is imposed at the capping inversion level $z = 0.3$ m.

For case III we consider an experimental setup with enhanced surface roughness (ER). The roughness length of the underlying heated surface is increased by the factor of 10 compared with the BFC (see FNK1), up to the value 0.001 m.

In addition to the three configurations specified above, other flow cases have been investigated. An example is a configuration with increased stability in the outer flow region. This configuration is indicated in Fig. 1 as IG. In this case, the temperature gradient above the inversion in the incoming flow is twice the value of the BFC and set equal to 66 K m^{-1} (10 K $layer^{-1}$ in the wind tunnel). This increase of hydrostatic stability in the outer flow corresponds approximately to the growth by the factor of 2 of the Richardson number $\mathrm{Ri}_N = \beta(dT/dz)z_i^2 w_*^{-2}$, which characterizes the damping of convection by stable stratification above the inversion. However, both the numerical simulations and the wind tunnel experiments indicated no significant effect of such increased outer-flow stability on the mean flow characteristics and turbulence statistics in the CBL within the investigated range of Ri_N numbers. Only small alterations have been observed in the mean temperature profiles close to the inversion base and in the temperature variances inside the inversion layer. These variances have been slightly larger in the IG case compared to the BFC.

Therefore, in the subsequent sections of the paper we will limit ourselves to a discussion of the laboratory and numerical results for the cases I, II, and III only.

All three flow configurations have been investigated numerically. Wind tunnel experiments have been performed for the cases I (PS) and III (ER). Unfortunately, the tunnel in its present state cannot be used for modeling the CBL with negative elevated shear due to the spurious accumulation of heat above the inversion under conditions of strong entrainment; see details of the tunnel design in Rau and Plate (1995), and discussion in Fedorovich et al. (1996). The results of wind tunnel and numerical experiments will be presented in the following sections, where we discuss first the effects of positive and negative shear and then the effect of increased roughness.

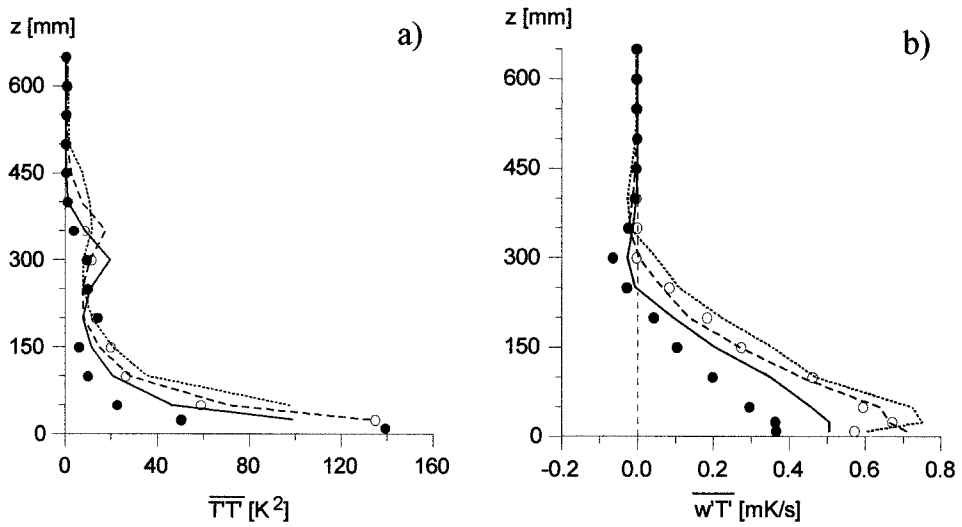

FIG. 2. Temperature variance (a) and vertical kinematic heat flux (b) measured in the wind tunnel CBL with positive shear across the inversion (PS case, points) and without shear (BFC, lines). Data refer to $x = 3.98$ m (solid lines and black symbols), $x = 5.63$ m (dashed lines and gray symbols), and to $x = 7.28$ m (dotted lines and empty symbols).

3. Effects of elevated shear

The wind tunnel data on the temperature variance and vertical kinematic heat flux for the case of positive elevated shear (PS) are presented in Fig. 2. These turbulence statistics show the effect of shear on the entrainment and the CBL growth in the most illustrative way. Data on some other turbulence statistics referring to the PS case can be found in Fedorovich and Kaiser (1998).

The heat flux minimum within the inversion is often taken as indicator of the CBL upper interface (Deardorff 1970; Fedorovich and Mironov 1995). The maximum of the temperature variance inside the inversion layer can be also used for identification of the CBL top (Fedorovich et al. 1996). Based on these two criteria, one can clearly see in both plots of Fig. 2 the progressive growth of the CBL depth as a function of x in the case without elevated shear (BFC). In the case of imposed positive shear (PS), the CBL depth does not significantly vary along the tunnel as may be inferred from practically constant elevations of both heat flux minima and temperature variance maxima. Therefore, we conclude that positive elevated shear leads to a slower CBL deepening than in the case of CBL with a shear-free upper interface.

The blocking effect of shear on the turbulence propagation across an interface separating turbulent and turbulence-free flow regions has been theoretically analyzed by Hunt and Durbin (1999). They have used for this effect the term ''shear sheltering.'' According to analysis of Hunt and Durbin, the rms amplitude of the normal component of the induced velocity fluctuations across the interface, $\overline{w_n'^2}^{1/2}$, relative to the characteristic value of velocity perturbation in the turbulent flow, u_t, which one may call the sheltering ratio, is given by

$$\frac{\overline{w_n'^2}^{1/2}}{u_t} \equiv R_s = C_I \frac{|\Delta U^2/4 - c_r^2|}{|\Delta U^2/4 + c_r^2|}, \tag{1}$$

where $\Delta U = U_t - U_n$ is the mean velocity shear across the interface (subscripts t and n stand for the turbulent and nonturbulent flow regions, respectively); C_I is the isotropy coefficient, which is assumed to be a positive constant; and

$$c_r = c - U_s = c - (U_t + U_n)/2 = c - U_t + \Delta U/2 \tag{2}$$

is the speed of perturbation transport in the turbulent flow relative to the average velocity in the interface, $U_s = (U_t + U_n)/2$. The quantity c denotes the traveling speed of a perturbation in the turbulent flow region. It follows from the above expressions that with $c = U_t$, which corresponds to $c_r = \Delta U/2$, the shear totally shelters the turbulence-free fluid from the perturbations: $\overline{w_n'^2}^{1/2}/u_t = 0$. With the speed of perturbation transport different from U_t, the relative value of rms amplitude of the induced velocity fluctuations varies in the range from 0 to C_I. The latter limit is achieved when either $\Delta U = 0$ or $c = U_s$.

If for a moment we disregard the stable temperature gradient across the upper interface of the wind tunnel CBL, we may use Eqs. (1) and (2) to estimate the net contribution of shear to the damping of buoyancy induced perturbations (thermals) by the shear layer at the CBL top. Flow visualizations in the tunnel show that thermals, which originate from the heated surface with zero horizontal velocity, are eventually transported in the bulk of the CBL with velocity c that is slightly smaller than the mean flow velocity $U_t = 1$ m s^{-1}. Let us therefore as a first guess take $c = 0.9U_t$. If we further

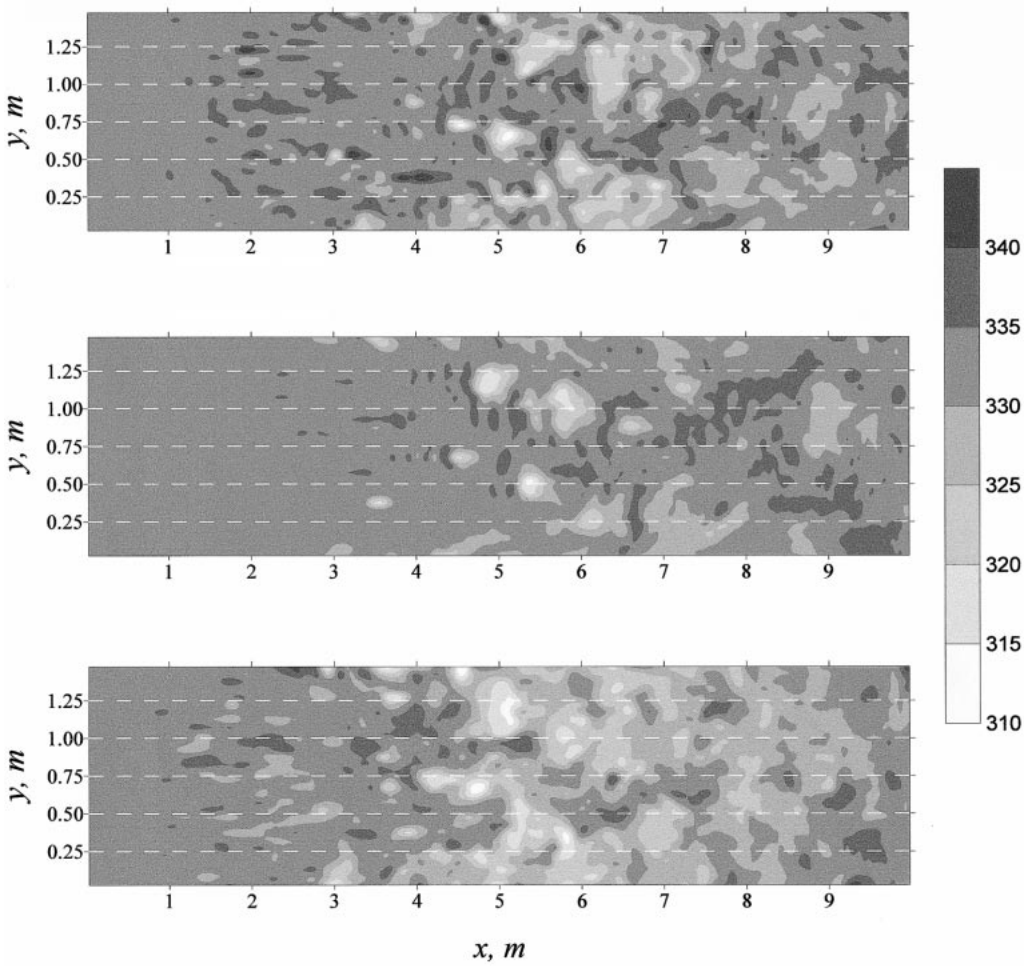

FIG. 3. Simulated instant temperature distributions over horizontal planes inside the inversion layer, at $z = 0.375$ m. The uppermost plot corresponds to the BFC, the middle plot to the PS case, and the lowest plot to the NS case.

assume $C_I \approx 1$ and $\Delta U = U_t - U_n = -0.5$ m s^{-1}, we obtain estimates of the relative transport velocity $c_r = -0.35$ m s^{-1}, and of the shear sheltering ratio $R_s \approx 0.32$. The estimation with $c = 0.8U_t$ leads to $c_r = -0.45$ m s^{-1} and $R_s \approx 0.53$.

Both these estimates are in qualitative agreement with the earlier discussed wind tunnel data (see Fig. 2) pointing to the impedance of vertical turbulent transport across the inversion in the case of CBL with positive elevated shear as compared to the case of CBL with the shear-free upper interface.

The LES results for the PS case have provided an additional confirmation for these wind tunnel experimental data. In Fig. 3, the numerically simulated instantaneous temperature distributions are shown over horizontal planes within the inversion layer. All presented patterns refer to the same elevation above the surface. One may easily notice the obstruction of penetration of the cooler and less buoyant air from the mixed layer into the stably stratified fluid in the PS case compared to the BFC with a shear-free interface. The total area occupied by the mixed-layer air (colored white and light gray) in the PS case (middle plot) is reduced to almost half compared to the case with shear-free inversion (upper plot).

The LES experiments with negative shear across the inversion layer (the NS case; the mixed-layer air has a higher momentum than the air above the inversion) yield quite different and rather unexpected results. It turns out that in this case the damping of thermals in the inversion layer is weakened compared to the BFC and as a result the entrainment is activated. The effect of negative elevated shear on the CBL growth is thus opposite to that of the positive shear. The lowest plot in Fig. 3 clearly demonstrates the intensification of vertical transport of air from the mixed layer into the above-inversion flow region in the NS case.

This result for the NS case is in contradiction with the analysis of Hunt and Durbin (1999). Their theory predicts that, apart from particular cases such as $\Delta U = 0$ and $c = U_s$, a sheared interface always produces some sheltering effect independent of the direction of shear

across the interface. Hence, according to the theory of Hunt and Durbin, the effect of shear can never lead to any amplification of perturbations at the interface, or R_s cannot be larger than C_I. For instance, in the NS case, taking $U_t = 1$ m s^{-1}, $c = 0.9\ U_t$, $C_I \approx 1$, and $\Delta U = 0.5$ m s^{-1}, we obtain for R_s an estimate 0.47.

One may suspect that the reason for this inconsistency between theory and simulation results lies in the neglecting by the theory of the role of density stratification and turbulence structure. This will be discussed further in the last section of the paper, where we consider possible physical mechanisms of directional effect of wind shear on the turbulent transport across the inversion layer. Here, we continue by presenting additional data on the CBL flow characteristics and turbulence statistics for the cases of positive and negative elevated shear as derived from the LES. The results are presented in Figs. 4–7. The data summarized in the plots refer to the CBL downwind of the transition zone that has been discussed in FNK1.

Profiles of the horizontal velocity shown in Figs. 4a (the PS case) and 4b (the NS case) refer to three measurement locations in the tunnel (the wind tunnel windows 3 to 5; see Fedorovich et al. 1996). As reference, the BFC u profiles in the same locations are also given. Considerably larger velocity gradients at the CBL top in the first plot make clear that turbulent exchange of momentum across the inversion is much weaker in the PS case than in the NS case. It is also clear that the propagation of turbulence inside the initially quiescent flow above the CBL is relatively faster in the NS case. This growth is accompanied by active entrainment of

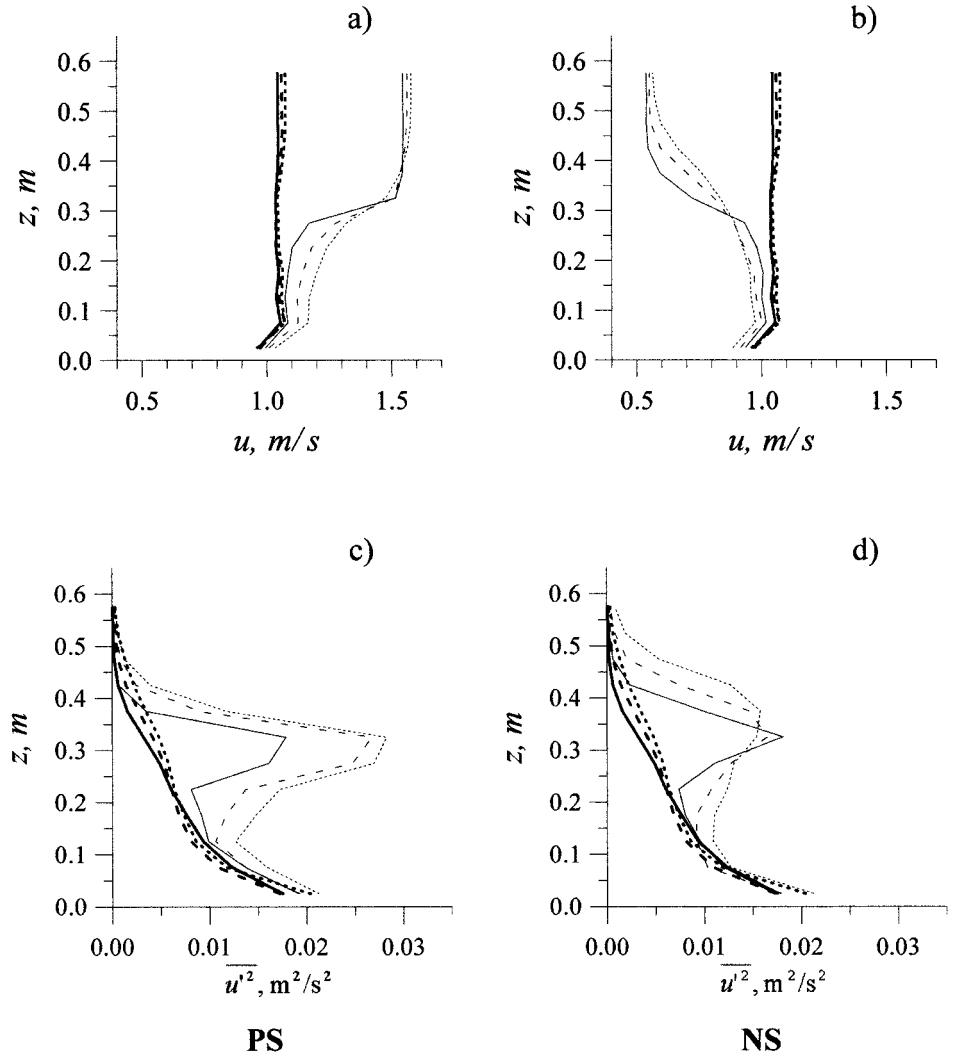

FIG. 4. Mean flow values (a), (b) and variances (c), (d) of the longitudinal velocity component in three subsequent locations along the simulation domain: $x = 3.98$ m (solid lines), $x = 5.63$ m (dashed lines), and $x = 7.28$ m (dotted lines). Simulation data for the cases with elevated shear (PS and NS) are presented by thin lines. The corresponding BFC profiles are shown for comparison by heavy lines.

momentum downward into the mixed layer. The entrainment of momentum is practically absent in the CBL with positive shear across the capping inversion. In this case, turbulent perturbations from the mixed layer do not significantly penetrate above the inversion and all changes of the velocity field happen below the inversion. We will see later in Figs. 6c and 6d that the magnitude of the entrainment momentum flux close to the CBL top is very small in the PS case compared to its counterpart in the NS case.

One should keep in mind that the magnitudes of the inlet velocity increments across the inversion for the cases PS and NS are the same. The temperature increments in the incoming flow for these two cases are equal. This means that the observed differences in turbulence dynamics at the inversion level are solely associated with the sign of shear-induced transport of momentum across the inversion.

Alterations in the streamwise velocity variance by the elevated wind shear are shown in Figs. 4c (PS case) and 4d (NS case). The positive shear produces asymmetric maxima in the $\overline{u'^2}$ profiles at the level of the inversion. The maxima referring to different fetches are located practically at the same height. The magnitudes of these maxima are growing with x thus suggesting that the kinetic energy of thermals destroyed at the inversion level by shear and stable stratification is transferred to horizontal velocity fluctuations. Beyond the maximum, the u variance values drops sharply to a small value in the stably stratified flow region. This fast decay of $\overline{u'^2}$ above the mixed layer provides support for the wind tunnel observation of turbulence blockage due to shear sheltering in the CBL with positive elevated shear.

In the NS case (Fig. 4d), the decrease of longitudinal velocity variance within the inversion is more gradual. The $\overline{u'^2}$ maximum broadens and shifts upwards with a growing fetch, but its magnitude remains unchanged. The deepening of the turbulent flow region in this case is noticeably faster than in the BFC, not to speak about the PS case, where the vertical extension of the turbulent zone is practically constant (compare $\overline{u'^2}$ profiles in Figs. 4d and 4c).

This opposite effect of positive and negative elevated shear on the CBL development is most clearly seen in the vertical distribution of the temperature variance (Figs. 5a and 5b) and of the kinematic heat flux (Figs. 5c and 5d). Both the maximum of $\overline{T'^2}$ and the minimum of $\overline{u'T'}$, which roughly define the position of the capping inversion, are found below the corresponding BFC extrema in the PS case and above them in the NS case. The magnitudes of temperature variance and negative heat flux of entrainment inside the inversion layer are not significantly altered in the PS and NS cases compared to their reference values in the BFC.

The obstruction of vertical motions in the CBL capped with positive shear, and—oppositely—their enhancement in the NS case may be assessed also from the vertical distributions of $\overline{w'^2}$ shown in Figs. 6a and 6b.

In the PS case, the vertical transport of momentum vanishes relatively fast inside the sheared inversion layer close to the CBL top, (see Fig. 6c), and the turbulent momentum flux is negative throughout the whole boundary layer. The corresponding momentum flux variation with height below the inversion is rather small. This is not the case in the CBL with negative elevated shear (Fig. 6d). Here, the momentum flux, which is negative near the surface, reaches its zero-crossing height roughly in the middle of the mixed layer and gains toward the CBL top approximately the near-bottom magnitude but with a positive sign. Above the inversion, the momentum flux gradually decreases with height to zero. The vertical distribution of the turbulent momentum flux for the NS case provides additional evidence of the amplification of vertical turbulent exchange at the inversion level compared to the BFC. We have already reached a similar conclusion based on the profiles of kinematic heat flux (Fig. 5d).

The LES data on the vertical velocity and temperature skewness in the CBLs with positive and negative elevated shear are summarized in Fig. 7. In the PS case (Fig. 7a), one may observe the general decrease of w skewness at the inversion level compared to the BFC. This is a sign of weaker and wider upward motions in the upper portion of CBL with positive elevated shear. With negative elevated shear (Fig. 7b), the vertical velocity skewness at the inversion base level has approximately the same values as in the BFC. However, it drops relatively fast throughout the inversion down to near-zero values. This suggests that in the NS case the updrafts and downdrafts play approximately equal roles in the enhanced vertical turbulent exchange at the CBL top.

The temperature skewness values in the both cases with elevated shear (Figs. 7c and 7d) do not show clear deviations from quite scattered values of T skewness found in the BFC. Nevertheless, one may note that temperature distribution above the inversion in the PS case is negatively skewed while the temperature fluctuations in the NS case have practically zero skewness. Such negative skewness values in the former case may be associated with the handicapped heat exchange at the CBL top due to the damping effect of positive shear. From the other side, stronger turbulent transport at the inversion level in the NS case leads to the approximate symmetry of temperature distribution in the upper portion of the CBL.

4. Effects of increased surface roughness

In contrast to the effects of elevated shear, which are localized in the upper portion of the CBL, the effects of enhanced bottom roughness (the ER case in Fig. 1) are distributed over the whole CBL depth. This is clearly demonstrated by velocity variance distributions derived

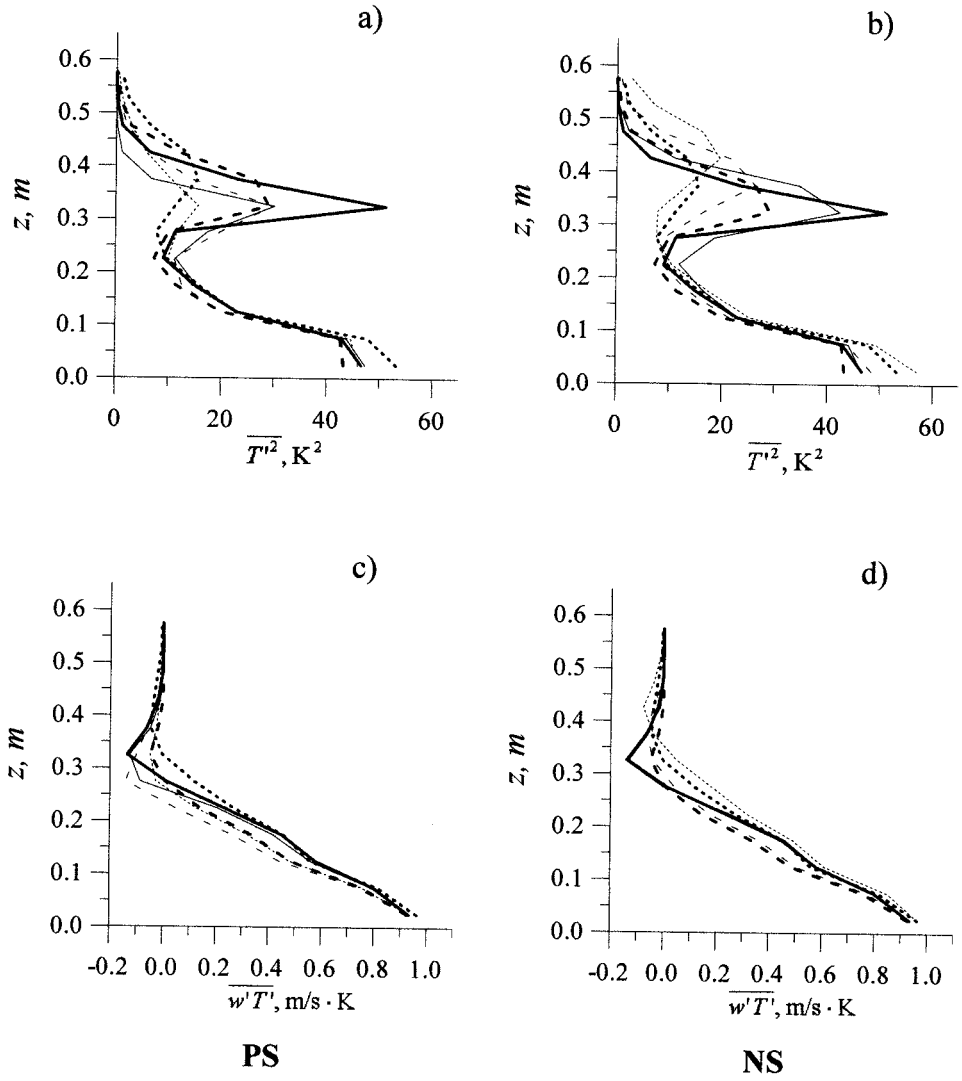

FIG. 5. Temperature variance (a), (b) and vertical kinematic heat flux (c), (d) in three subsequent locations along the simulation domain for the cases PS and NS. For notation see Fig. 4.

from the wind tunnel measurements. They are shown in Fig. 8.

Compared to the BFC, both u and w variances are somewhat increased in the ER case. The effect of enhanced roughness is primarily found in the increase of the horizontal velocity variance (Fig. 8a). One may notice that a bigger roughness leads to the larger variability of velocity variances along the tunnel. Local amplification of the velocity fluctuations associated with transition (see discussion in FNK1) is also stronger in the ER case. This is illustrated by larger differences between velocity variances at $x = 3.98$ m and subsequent locations in the ER case compared to the same locations in the BFC. Vertical distributions of both u and w variances provide evidence of slightly larger CBL growth rate over the rougher surface (ER case) than over the comparatively smooth floor (BFC).

Numerical results for the ER case agree reasonably well with the wind tunnel data. They also show that enhanced roughness primarily affects the horizontal velocity component and only slightly modifies the regime of the vertical velocity fluctuations. The location of the transition zone, which is mainly determined by efficiency of the vertical mixing (see FNK1), is practically the same in the ER case as in the BFC. Simulated instant distributions of u along the tunnel (Fig. 9) demonstrate that in both cases transition happens within the fetch range from 3 to 5 m. However, the horizontal variability of longitudinal velocity component is much larger in the ER case. Such variability is related to the intensified mechanical production of horizontal velocity fluctuations due to interaction of the flow with comparatively large roughness elements.

Due to the increased roughness, the surface friction in

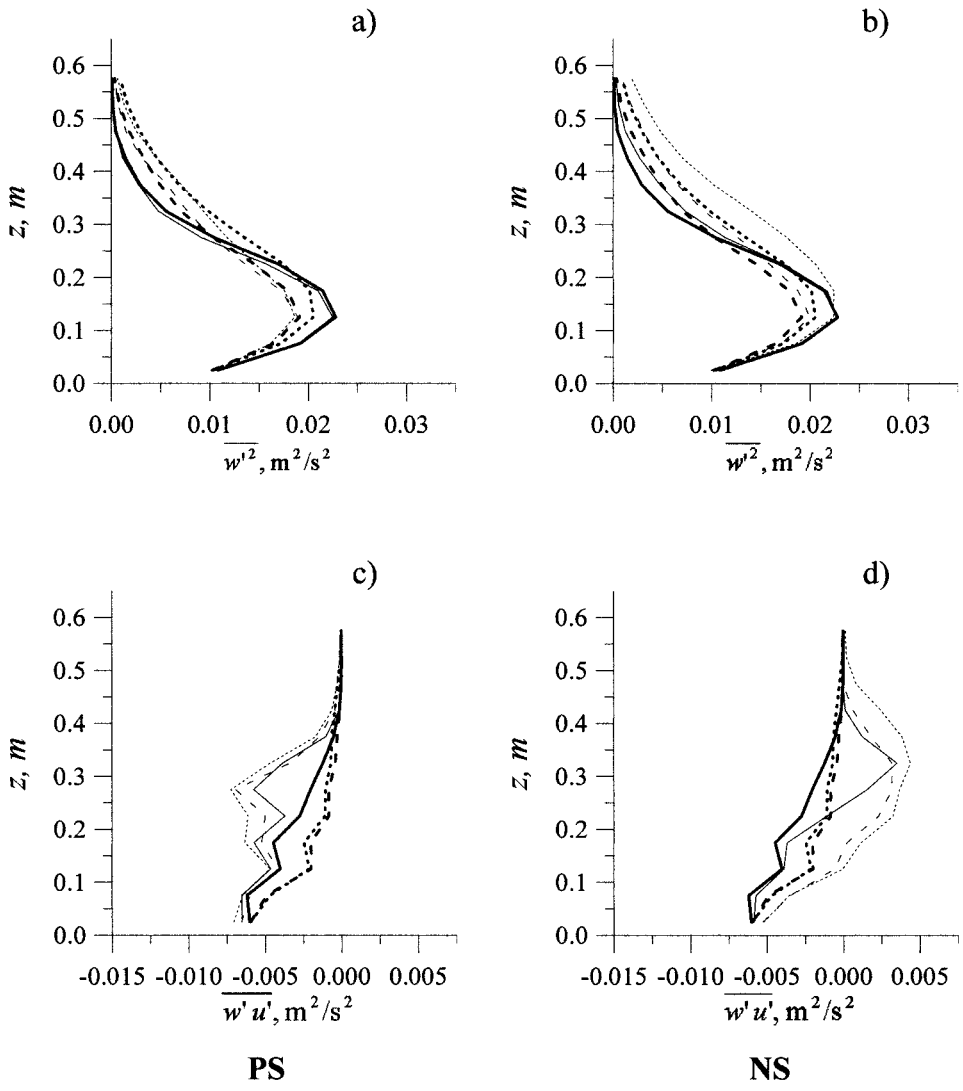

FIG. 6. Vertical velocity variance (a), (b) and vertical turbulent flux of momentum (c), (d) in three subsequent locations along the simulation domain for the cases PS and NS. For notation see Fig. 4.

the ER case is stronger and, consequently, the mean flow below the inversion in this case is slower than in the BFC. This deceleration of the flow below the inversion is illustrated in Fig. 10a, where calculated u profiles for the ER case are compared with their BFC counterparts. Differences between the two cases with respect to the vertical transport of momentum are illustrated in Fig. 10b. In the ER case, with a surface roughness length 1 order of magnitude larger than in BFC, the magnitude of the turbulent kinematic momentum flux near the surface is roughly 3 times larger than at the same locations in the BFC. In both cases, the largest magnitudes of momentum flux are observed in the downwind region of transition zone, at $x = 3.98$ m.

Other turbulence statistics derived from the LES also behave rather peculiarly in the vicinity of transition zone. The u and w variances (Figs. 10c and 10d) are markedly larger at $x = 3.98$ m than in the well-developed CBL downstream. The vertical distributions of variances obtained from LES at this fetch are very close to the ones measured in the tunnel (Figs. 8a and 8b). Both the wind tunnel experiment and LES show here a relatively shallow but rather turbulent CBL. In the developed CBL, at $x = 5.63$ m and $x = 7.28$ m, the wind tunnel and LES data on the turbulence enhancement by increased surface roughness continues to be in good agreement. The turbulence statistics from LES generally support the experimental observation that in the case of enhanced surface roughness the depth of the CBL grows faster. Evolution of the temperature variance profile in the ER case provides additional support for this observation, see Fig. 11a. The temperature variance values above the $\overline{T'^2}$ maxima, which mark the inversion layer, decrease noticeably slower with height in the ER case than in the BFC.

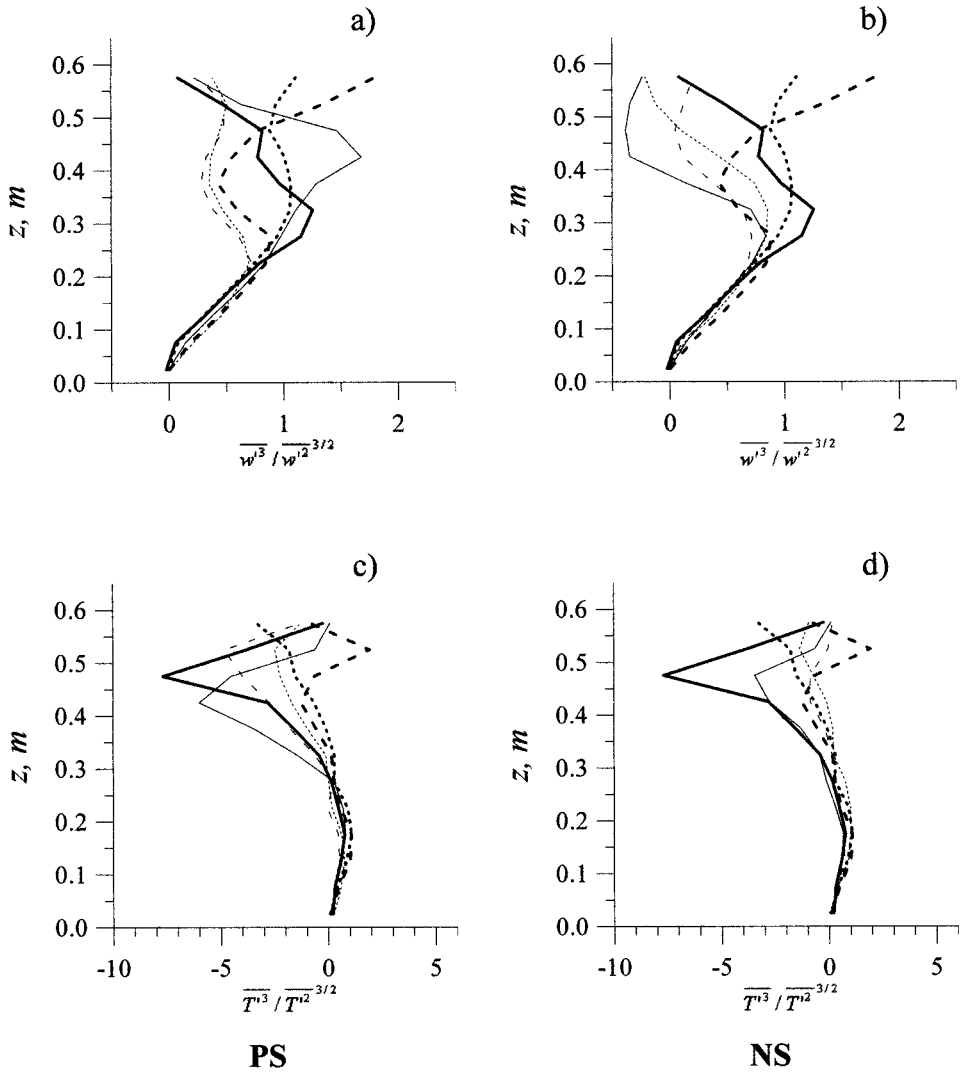

FIG. 7. Vertical velocity (a), (b) and temperature (c), (d) skewness in three subsequent locations along the simulation domain for the cases PS and NS. For notation see Fig. 4.

5. Discussion and conclusions

In the reported study, modifications of CBL turbulence by a number of nonbuoyant forcings have been investigated both numerically, by means of LES, and experimentally, in the UniKa thermally stratified wind tunnel. The emphasis has been laid on evaluation of the effects of surface friction and elevated wind shears on the momentum and heat transport within the bulk of the CBL, and across the capping inversion. For the flow cases, for which both numerical simulation and wind tunnel data have been available, the numerical results on mean flow parameters and turbulence statistics have been found to be in good agreement with the experimental results.

In the case of positive wind shear across the inversion layer (the flow above the inversion possesses a larger momentum than mean motion in the mixed layer), the CBL growth has been found to be impeded compared to the shear-free case. This result is in qualitative agreement with theoretical analysis of shear sheltering by Hunt and Durbin (1999). The entrainment of momentum into the CBL capped with positive shear layer has been found to be negligible. Practically all changes of mean flow velocity in the process of CBL development have been constrained to the mixed-layer flow region below the sheared inversion. The longitudinal velocity variance in the inversion layer with positive shear has displayed pronounced asymmetric maxima that have been growing downwind. This implies that in this case the kinetic energy of thermals, which are destroyed by shear and stable stratification within the inversion layer, is primarily redistributed into horizontal velocity fluctuations whilst the penetrability of thermals in the vertical direction is obstructed.

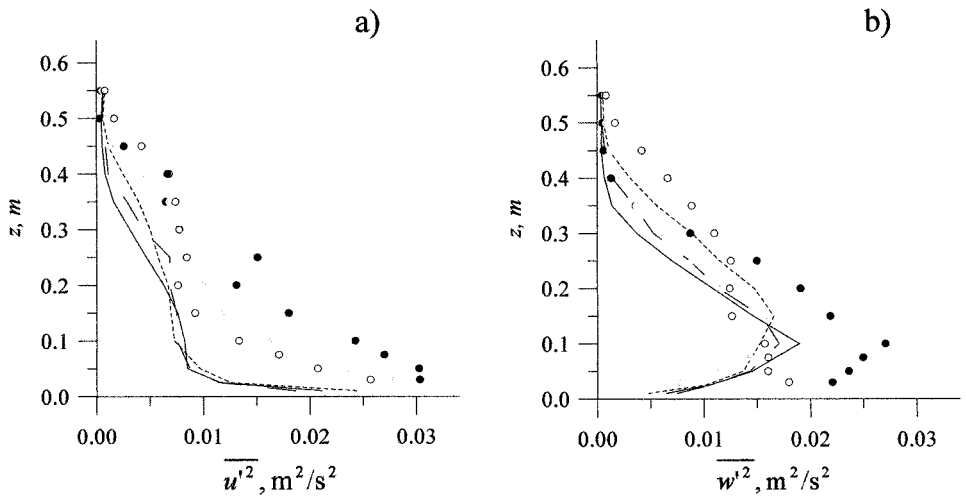

FIG. 8. Longitudinal (a) and vertical (b) velocity variances measured in the wind tunnel CBL with different surface roughness lengths. Profiles for the BFC (smaller roughness) are shown by lines. Points represent the ER case (bigger roughness). Data refer to $x = 3.98$ m (solid lines and black symbols), $x = 5.63$ m (dashed lines and gray symbols), and to $x = 7.28$ m (dotted lines and empty symbols).

The LES experiments with negative shear across the inversion layer (the flow above the inversion possesses a smaller momentum than mean motion in the mixed layer) have led to quite unexpected results. It turns out that in this case the damping of thermals by stable stratification in the inversion layer is weakened compared to the shear-free case and thus the entrainment is activated. In this way, the effect of negative elevated shear on the CBL growth has been found to be opposite to that of the positive shear. This finding does not agree with the theory of shear sheltering by Hunt and Durbin (1999) which predicts shear sheltering to be independent of the sign of shear. However, this theory does not take into account the effects of stratification and turbulence structure on the penetration of turbulent disturbances through the sheared layer. These effects may be relevant in the case of CBL with sheared capping inversion.

We are not aware of any field, laboratory, or numerical CBL studies, where the discovered directional effect of the elevated wind shear on the turbulent exchange across the capping inversion has been investigated or described.

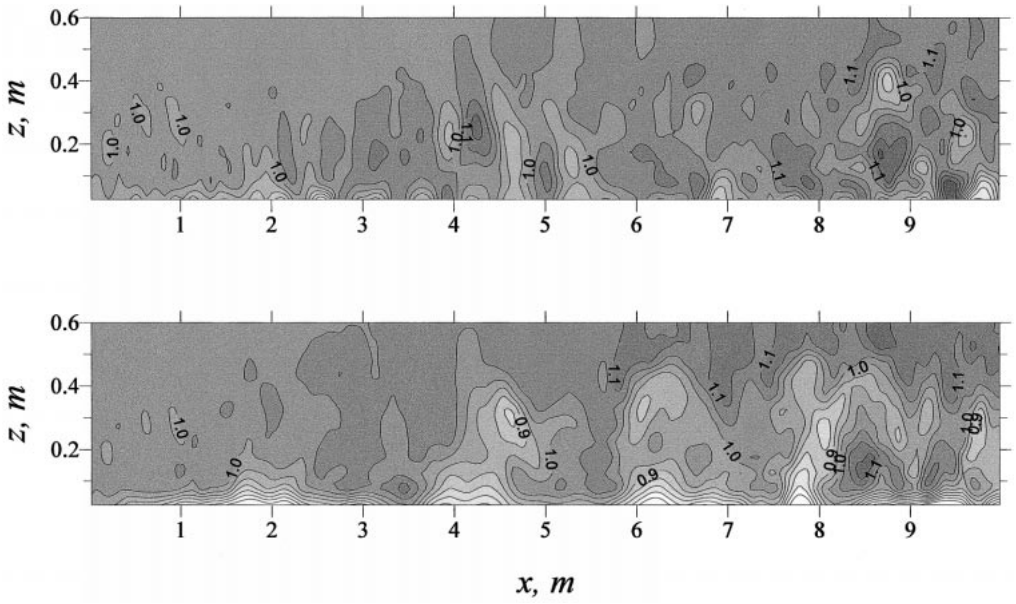

FIG. 9. Simulated instant distributions of longitudinal velocity along the central plane of the tunnel for the cases BFC (upper plot) and ER (lower plot). (Velocity values are given in m s^{-1}.)

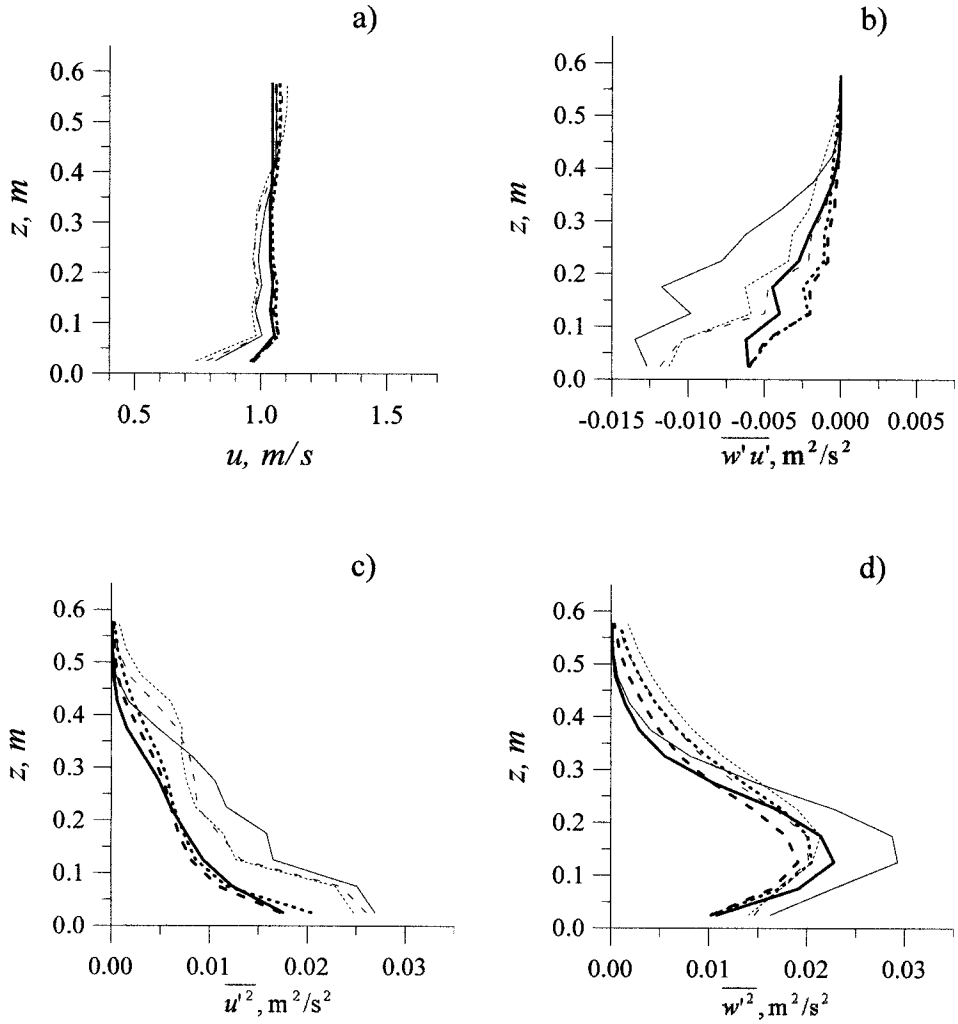

FIG. 10. Mean-flow values of longitudinal velocity (a), vertical turbulent momentum flux (b), and longitudinal (c) and vertical (d) velocity variances in three subsequent locations along the simulation domain: $x = 3.98$ m (solid lines), $x = 5.63$ m (dashed lines), and $x = 7.28$ m (dotted lines). Thin lines show simulation results for the ER case, and heavy lines correspond to the BFC.

Our wind tunnel and numerical results suggest that directional character of this effect follows from three particular features of the turbulence regime in the CBL. The first is the dominance of buoyant forcing in the production of CBL turbulence. This forcing leads to strongly anisotropic turbulence patterns, where the vertical turbulent motions dominate the horizontal ones. The second feature is the difference in scales and energy between the upward and downward components of turbulent motion in the CBL. The former component is represented by narrow and fast rising thermals while the latter one takes the form of broad and slow downdrafts. The third feature is the interaction of rising thermals with the capping inversion and stably stratified fluid above it. This interaction is associated with the erosion of inversion, destruction of thermals, and entrainment of buoyant air from above the inversion down into the mixed layer.

Therefore, the dynamics of CBL growth is essentially determined by transformations of energy and momentum carried by rising thermals. When the thermals penetrate in the inversion layer, a part of their kinetic energy is spent on work against the buoyancy force. Another part is transformed into kinetic energy of the downward entraining motions. Both these transformations result in the mixing of air within the inversion and, consequently, in the progressive CBL growth.

With positive elevated shear, the thermals, which penetrate into the sheared inversion layer are vertically squashed by the stable stratification and additionally stretched downwind by the higher-momentum flow in the inversion layer. This stretching leads to the locali-

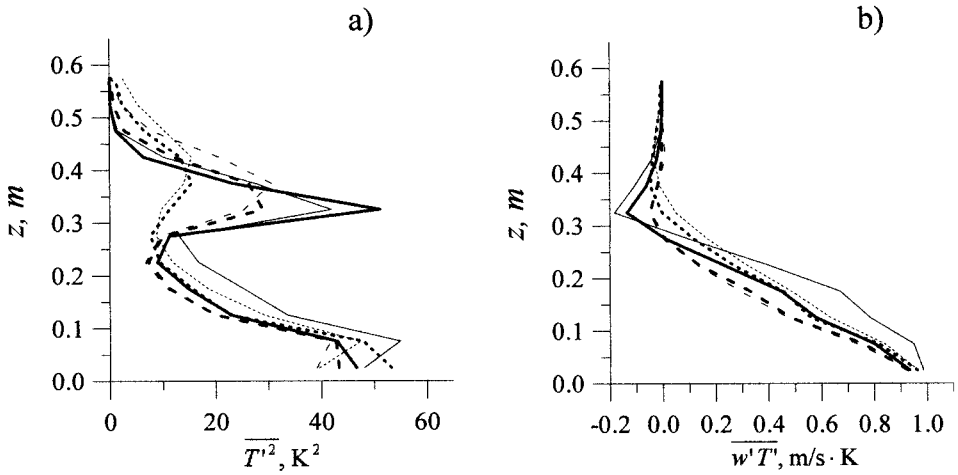

FIG. 11. Temperature variance (a) and vertical turbulent kinematic heat flux (b) in three subsequent locations along the simulation domain for the ER case. For notation see Fig. 10.

zation of vertical motion within a comparatively shallow zone and, consequently, to the reduction of vertical turbulent exchange across the inversion layer. As we have seen from the wind tunnel and LES results, the convective entrainment in this case is handicapped compared to the CBL with shear-free inversion. Apparently, the downward entraining motions within the inversion layer are also affected by the elevated shear. In view of the results found for the negative shear case, one may expect that in this case the effect should be opposite to the shear effect on the rising thermals. However, due to the secondary character of downward motions, (as was mentioned above, the energy they carry is merely a fraction of the energy of thermals), their modification by shear may be considered insignificant compared to its effect on the rising thermals.

With negative elevated shear, the penetrating thermals are also squashed vertically by the stable stratification. However, in this case they additionally encounter a lateral blockage by the lower-momentum flow, which brakes their horizontal transport. Such blockage induces local pressure gradients that redistribute energy from the horizontal velocity component to the vertical one. The enhanced vertical motions intensify the turbulent exchange across the inversion and provide a stronger entrainment in the NS case than in the CBL without elevated shear. This could be a possible physical mechanism of entrainment amplification in the CBL with negative shear which we have observed in the patterns of turbulence statistics from the LES.

In addition to statistical analysis of the flow fields derived from the LES, the simulated velocity and temperature fields have been visualized over the central longitudinal plane of the computational domain. These visualizations have shown that in the PS case the warm updrafts (thermals) are distorted and slanted downstream once they reach the sheared inversion layer, with their penetrability being noticeably hampered compared to the shear-free case. In the NS case, on the contrary, the thermals that have gained a horizontal momentum in the mixed layer are somehow reerected when they encounter the slower flow beyond the inversion base. This makes them more efficient in penetrating into the stably stratified fluid than their counterparts in the shear-free case.

The disturbances of the CBL turbulence regime induced by enhanced bottom roughness have been found to affect the entire depth of the CBL. Both horizontal and vertical velocity variances have been enlarged compared to the reference case with 1 order of magnitude smaller roughness. Besides this increase in turbulence, the larger longitudinal variability of velocity variances and stronger transition effects have been identified in the flow over the rougher surface. Vertical profiles of CBL turbulence statistics from the wind tunnel model and LES have given an indication of slightly higher CBL growth rate over the underlying surface with the roughness enhanced by the factor of 10.

Acknowledgments. Financial support provided for the study by the Deutsche Forschungsgemeinschaft (DFG) within the Project ''Untersuchung und Parametrisierung der Wechselwirkungen von Skalen der Turbulenz konvektiver Grenzschichtströmungen unter Verwendung einer einheitlichen Datengrundlage aus Naturmessungen, Windkanalversuchen und numerischen Modellen'' is gratefully acknowledged. The authors are grateful to Julian Hunt for his constructive interest to the study, and to Johannes Thäter for the technical assistance in visualization of the LES results.

REFERENCES

Cai, X.-M., 1999: Large-eddy simulation of the convective boundary layer over an idealized patchy urban surface. *Quart. J. Roy. Meteor. Soc.,* **125,** 1427–1444.

Deardorff, J. W., 1970: Convective velocity and temperature scales for the unstable planetary boundary layer and for Raleigh convection. *J. Atmos. Sci.,* **27,** 1211–1213.

Fedorovich, E., 1995: Modeling the atmospheric convective boundary layer within a zero-order jump approach: An extended theoretical framework. *J. Appl. Meteor.,* **34,** 1916–1928.

——, 1998: Bulk models of the atmospheric convective boundary layer. *Buoyant Convection in Geophysical Flows,* E. J. Plate et al., Eds., Kluwer, 265–290.

——, and D. V. Mironov, 1995: A model for shear-free convective boundary layer with parameterized capping inversion structure. *J. Atmos. Sci.,* **52,** 83–95.

——, and R. Kaiser, 1998: Wind tunnel model study of turbulence regime in the atmospheric convective boundary layer. *Buoyant Convection in Geophysical Flows,* E. J. Plate et al., Eds., Kluwer, 327–370.

——, ——, M. Rau, and E. Plate, 1996: Wind-tunnel study of turbulent flow structure in the convective boundary layer capped by a temperature inversion. *J. Atmos. Sci.,* **53,** 1273–1289.

——, F. T. M. Nieuwstadt, and R. Kaiser, 2001: Numerical and laboratory study of horizontally evolving convective boundary layer. Part I: Transition regimes and development of the mixed layer. *J. Atmos. Sci.,* **58,** 70–86.

Holtslag, A. A. M., and F. T. M. Nieuwstadt, 1986: Scaling the atmospheric boundary layer. *Bound.-Layer Meteor.,* **36,** 201–209.

Hunt, J. C. R., 1998: Eddy dynamics and kinematics of convective turbulence. *Buoyant Convection in Geophysical Flows,* E. J. Plate et al., Eds., Kluwer, 41–82.

——, and P. A. Durbin, 1999: Perturbed vortical layers and shear sheltering. *Fluid Dyn. Res.,* **24,** 375–404.

Jacobs, R. G., and P. A. Durbin, 1998: Shear sheltering and the continuous spectrum of the Orr–Sommerfeld equation. *Phys. Fluids,* **10,** 2006–2011.

Kaiser, R., and E. Fedorovich, 1998: Turbulence spectra and dissipation rates in a wind tunnel model of the atmospheric convective boundary layer. *J. Atmos. Sci.,* **55,** 580–594.

Khanna, S., and J. G. Brasseur, 1998: Three-dimensional buoyancy- and shear-induced local structure of the atmospheric boundary layer. *J. Atmos. Sci.,* **55,** 710–743.

Mason, P. J., 1992: Large-eddy simulation of dispersion in convective boundary layers with wind shear. *Atmos. Environ.,* **26A,** 1561–1571.

Moeng, C.-H., and P. P. Sullivan, 1994: A comparison of shear- and buoyancy-driven planetary boundary layer flows. *J. Atmos. Sci.,* **51,** 999–1022.

Rau, M., and E. J. Plate, 1995: Wind tunnel modelling of convective boundary layers. *Wind Climate in Cities,* J. Cermak et al., Eds., Kluwer, 431–456.

Stull, R. B., 1988: *An Introduction to Boundary Layer Meteorology.* Kluwer Academic, 666 pp.

Sykes, R. I., and D. S. Henn, 1989: Large-eddy simulation of turbulent sheared convection. *J. Atmos. Sci.,* **46,** 1106–1118.

Wyngaard, J. C., 1998: Experiment, numerical modeling, numerical simulation, and their roles in the study of convection. *Buoyant Convection in Geophysical Flows,* E. J. Plate et al., Eds., Kluwer, 239–252.

Zilitinkevich, S., A. Grachev, and J. C. R. Hunt, 1998: Surface frictional processes and non-local heat/mass transfer in the shear-free convective boundary layer. *Buoyant Convection in Geophysical Flows,* E. J. Plate et al., Eds., Kluwer, 83–114.